Arch. Metall. Mater. **69** (2024), 3, 1079-1086

DOI: https://doi.org/10.24425/amm.2024.150928

K. SARAVANAKUMAR[1*], V.G. BALAJI[1], T. SRIJHA[1], V. SANJAY[1], K. THATCHUNESWARAN[1]

# ANALYSIS OF MICROSTRUCTURE AND MECHANICAL PROPERTIES OF INCONEL 625 ALLOY BY WIRE ARC ADDITIVE MANUFACTURING (WAAM)

An arc is used as a heat source in the manufacturing process known as wire arc additive manufacturing (WAAM), which uses layer-by-layer cladding to fuse wire. In the current work, Wire Arc Additive Manufacturing (WAAM)-fabricated Inconel 625 alloy has been examined. The research was done on the microstructure, mechanical characteristics, and impact of the solidification rate on the characteristics of the manufactured specimens for the Inconel 625 alloy. Microstructural analysis has shown that the specimen's layers have varying microstructures. The bottom layer exhibits a blocky or equiaxed microstructure because of the faster solidification rate, while the upper zone generated elongated and discontinuous dendrites because of the slower solidification rate. This difference in the microstructure in the top and bottom zones directly influence the ultimate tensile strength, where the bottom zone has more tensile and yield strength than the top zone. Also, the presence of cracks in the top zone, which is found during the fractography test, also correlated the top zone's ultimate tensile strength.

*Keywords:* Wire Arc Additive Manufacturing; optical microscope; multi-layered wall structure; fractography; tensile test

## 1. Introduction

A well-liked method for producing components with complicated shapes is Additive Manufacturing (AM), which greatly enhances production expertise and flexibility [1]. Recent developments have made it possible to use additive manufacturing (AM) to create fully dense parts with the best properties from industrial and engineering materials like aluminium, titanium, and steel [2]. The manufacturing sector is interested in Arc-welding-based additive manufacturing techniques due to their ability to compose large metal components at minimal cost and with a short processing lead time [3]. In order to melt and deposit the filler wire layer by layer to get the near-net structure component, WAAM uses an electrical arc as a heat source. For the WAAM method, weld filler wire has been used as the feedstock material. Additionally, the WAAM method demonstrated the feasibility of producing the large metallic component at a low cost [4]. There are three different types of WAAM processes, including Gas Tungsten Arc Welding (GTAW), Gas Metal Arc Welding (GMAW), and Plasma Arc Welding (PAW), depending on the type of heat source. Due to the fact that the electric current acts directly on the feedstock, GMAW has a deposition rate that is 2-3 times higher than that of GTAW or PAW, however, it produces more weld fumes and spatter [5]. When compared to GMAW or CMT-based additive manufacturing, the GTAW-based WAAM process allows direct control of the energy input and material input since changing the heat input does not affect arc length and changing the wire feed speed does not affect the deposition rate of GTAW based WAAM processing [6]. Multi-directional deposition is another distinction between GTAW WAAM and conventional automatic welding [7]. However, the qualities of weld produced by GTAW welding are influenced by several welding parameters, including welding current, voltage, polarity, gas flow rate, welding speed, and electrode tip angle [8]. The refractory metals present in a nickel-chromium matrix, such as niobium and molybdenum, have a solid-solution hardening effect that strengthens the nickel-based face-centered cubic super alloy Inconel 625 [9]. A study by Akselsen et al. [10], using the metal inert gas process' cold metal transfer, Inconel 625 was successfully wire arc additive manufactured. Heat input was between 0.46 and 0.63 kJ/mm, which is a negligibly low heat input and slow deposition rate. The results show that hardness increases from 210 for the base metal, to 220 for the heat-affected region (in the constructing plate) respectively, to 240-250 for the weld metal. However, using a pulsed TIG welding processing of Inconel 625 plates with activated flux, improves penetration

[1] PSG COLLEGE OF TECHNOLOGY, DEPARTMENT OF PRODUCTION ENGINEERING, COIMBATORE-641004, INDIA

* Corresponding author ksk.prod@psgtech.ac.in

up to 0.3 mm when V205 is used as flux and increases tensile strength by about 12% when $Al_20_3$ is used as flux. A study by Kumar S.S. [11] corroborate that using metal cored wire and the GTAW technique to deposit filler passes produced good results. When the WAAM-fabricated Inconel 625 alloy was tested on lab specimens, the microstructure revealed good forming quality, no flaws, and strong metallurgical bonding within the specimens. The predominant metallographic phases in the sample's cross-sections were Ni and granular precipitated phases, with average microhardness values of 243.5 and 243.3 HV 0.1 [12]. By using the WAAM process, a functionally gradient SS321/Inconel 625 material was also processed. While Inconel 625 has dendritic microstructures, the SS321 produced by WAAM has equiaxed and columnar structures. As a result an extremely narrow interface between the additively manufactured SS321/Inconel 625 FGM was created without any fissures or cracks [13]. The as-deposited alloy was discovered to have a columnar dendritic structure, and the gamma-nickel matrix contained intermetallic phases like the Laves phase, NbC, and carbides. It was discovered that the alloy's ultimate tensile strength and microhardness were greater than those of the as deposited weldments [13]. The mechanical characteristics of as-deposited and deposited materials alloys that have been solution-annealed (SA) were investigated by Ravi et al. [14]. At various temperatures ranging from 750°C to 1200°C, mechanical properties including hardness and tensile properties were examined. While the hardness varied irregularly with temperature, the ultimate tensile strength (UTS) increased from 193 MPa to 265 MPa moving from the bottom layer to the top layer [5]. Karayel E. et al. [15] explained about the introduction of AM technology and procedures. The method's application areas are described. Additionally, the effects of this new technique on the mechanical characteristics and microstructures as well as the welding parameters are examined. Ahmad G.N. et al. [16], have discussed a research on artterbium filament butt welding with Inconel 625 and Duplex stainless steel 2205 thin sheets. It is carried out utilizing the laser beam welding technique. Fiber laser beam welding may be used to create well- bonded, homogenous, and defect-free connections between the super alloys Inconel 625 and DSS 2205. Sivakumar J. et al. [17], described the welding process parameter optimization for 6.5 mm in thickness Inconel 625 plate using activated tungsten inert gas. To find the best values for the inputs, such as the impact of arc gap, torch travel speed, and welding current on penetration depth, the experimental design L25 has been used. Dhinakaran V. et al. [18], have reviewed on WAAM methods and the most widely used metallic feedstock materials and they concluded that the manufacture of large structural metallic components with moderate complexity with the wire-based AM method offers a low-cost, high efficiency, high-speed alternative to the powder-based AM technology.

According to the published results, choosing the right WAAM variables is crucial for producing multilayered wall components with useful mechanical and microstructural characteristics. The majority of WAAM Inconel 625 alloy studies used various substrate materials. Due to its thermal and chemical characteristic behavior, using a different material as a substrate will influence its mechanical and microstructural properties. The same Inconel 625 alloy material is used as the substrate in this study because the substrate plate is crucial to WAAM. In addition, the majority of studies used the GMAW process to perform WAAM. Because the GTAW process has advantages over the GMAW process, such as producing fewer splatters and higher-quality welds, it is crucial to develop GTAW process in WAAM. So, the study is conducted in GTAW process to build the weldment. Hence, in the current study, Inconel 625 alloy is welded using the GTAW welding process by WAAM method. From the weldment, specimens are generated from top and bottom zones. From the weldment, top and bottom zones produce specimens. By performing micro-hardness tests and tensile tests on the specimens, the mechanical properties are analysed. In order to identify the different phases and grain growths formed in the microstructure, the specimens are also subjected to microstructural analysis. Optical Microscopy (OM), and fractographic analysis are used to perform microstructural analysis.

## 2. Materials and methods

### 2.1. Experimental setup and plan

The WAAM process is done using a Gantry semi-automatic welding robot, coupled with a Fronius TPS 400i LSC ADV power source is shown in the Figs. 1(a) & 1(b) that was used to build the weldment using the GTAW process.

The base plate is subjected to Optical Emission Spectroscopy (OES) test to find out the elemental composition present in the plate. The elemental compositions present in the base plate are shown in the TABLE 1.

TABLE 1

Chemical composition of INCONEL 625 ALLOY

| Elements | C | Si | S | P | Mn | Cr | Mo | V | Cu |
|---|---|---|---|---|---|---|---|---|---|
| wt.% | 0.092 | 0.27 | 0.016 | 0.014 | 0.25 | 21.12 | 8.84 | 0.092 | 0.048 |
| **Elements** | **W** | **Ti** | **Co** | **Al** | **Nb** | **Fe** | **Ni** | **Ta** | |
| wt.% | 0.16 | 0.19 | 0.31 | 0.10 | 3.80 | 4.26 | 60.15 | 0.085 | |

To remove imperfections and assure a weld structure free of flaws, using the grinding machine, the substrate was machined, and acetone was used for cleaning. Current – 220 V, travel speed – 90 mm/min, and filler wire feed speed – 380 mm/min are the primary input parameters taken into account and the voltage was maintained upto 12 V-14 V. After setting the parameters, the plate is firmly mounted on the fixture to prevent distortion. The base metal is fused to form the molten pool using a non-consumable 3.2 mm diameter thoriated tungsten electrode. Inconel 625 alloy filler wire with a 1.2 mm diameter was deposited on the molten pool created in the base plate to build the thin-walled component using a GTAW process based on WAAM technology. During the deposition process, argon gas with a purity of 99.99% acts as

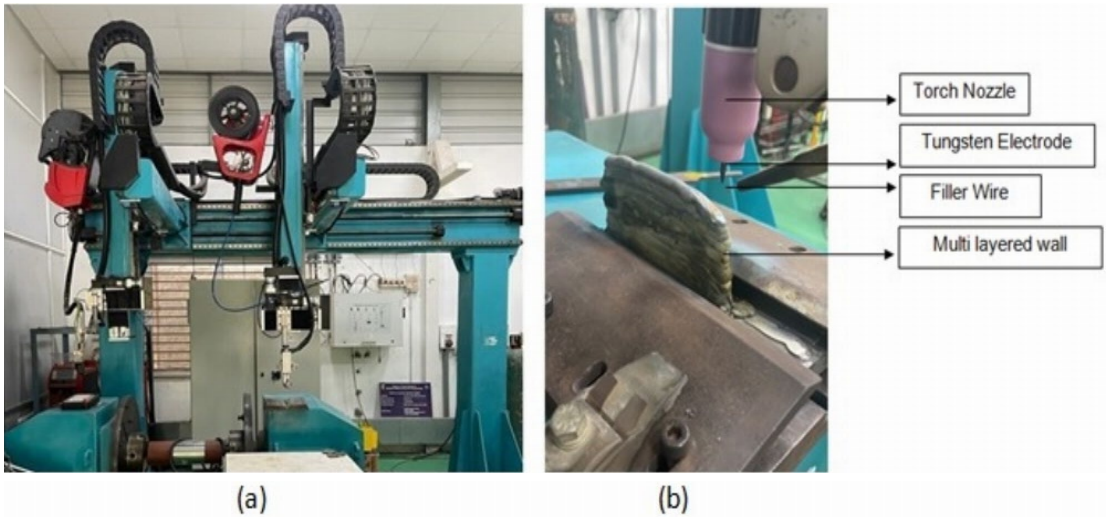


Fig. 1. (a) & (b) Experimental Setup of Semi-automatic GTAW Gantry welding robot

a shield with a flow rate of 15 L/min. After setting the parameters, the plate is firmly mounted on the fixture to prevent distortion. The thin, weldment is then constructed layer by layer using the chosen parameters. The interlayer temperature was lowered room temperature by maintaining a cooling time of 120 seconds between subsequent layer depositions. The constructed weldment with a 10 mm wall thickness and 66 mm height is shown in the Fig. 2.

### 2.2. Specimen preparation

Wire-cut EDM machining is used to remove the tensile coupons from the weldment in accordance with ASTM-E8 standards. Additionally, 10x10 mm specimens are taken out for micro hardness testing and microstructural analysis. For performing microstructural analysis, sample specimens are carefully polished and then electrolytically etched using 2.1 grams of oxalic acid mixed with 200 milliliters of distilled water connected to the DC power supply for 15 to 20 seconds.

### 2.3. Testing and characterization

The microstructure, mechanical characteristics, and fractography morphologies of the top and the bottom zones of the weldment were then studied.

In order to conduct a microstructural analysis, samples measuring 10 mm×10 mm are taken from the top and bottom zones of the weldment. By using coarse and fine grid emery sheets, the extracted samples are polished to a mirror-like finish without any visible scratch marks. While connected to the DC power supply, sample specimens are electrolytically etched for 15 to 20 seconds using 2.1 grams of oxalic acid and 200 milliliters of distilled water. Etched samples were examined microstructurally using an optical microscope in different magnifications to obtain the samples microstructures.

Mechanical properties like tensile test were conducted on the top and the bottom zones of the multilayered wall weldment. Tensile testing was performed according to the ASTM – E8 specification, utilizing a Universal testing machine (UTM), 600 KN. This test is used to find the tensile strength, yield strength and

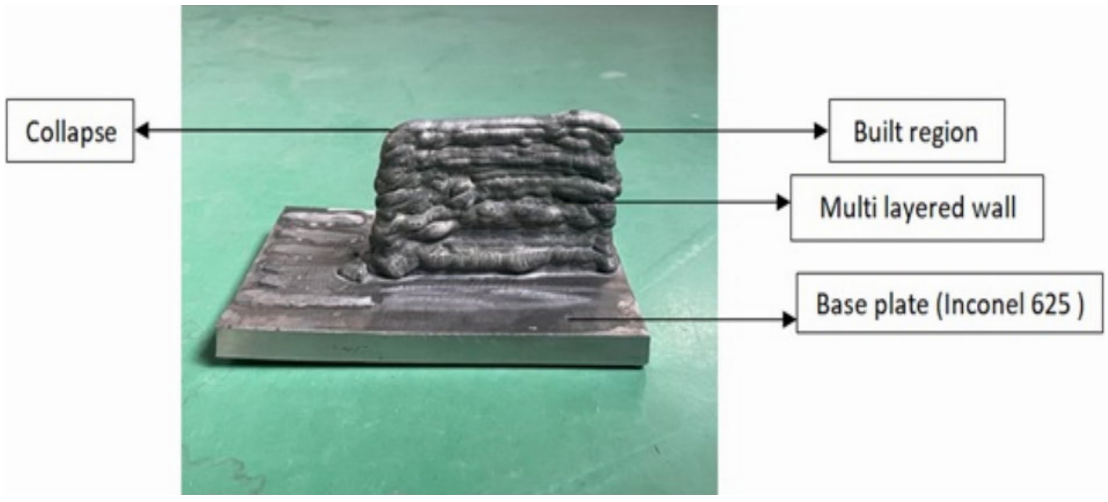


Fig. 2. Multilayer wall on INCONEL 625 ALLOY

ductility of the metallic material. The dimensions of the tensile specimen as per ASTM-E8 standard is shown in the Fig. 3. Also, in order to comprehend their characteristics more clearly of the fractured surface, the fractography test was examined in the SEM system on the fractured surface of the broken tensile specimen.

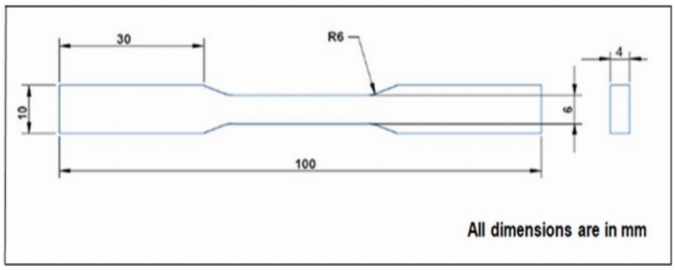


Fig. 3. Tensile specimen dimensions as per ASTM-E8 standard

## 3. Results and discussion

### 3.1. Appearance characteristics

The semi-automatic welding robot with the GTAW process uses WAAM to deposit the weldment, which has 42 layers and a height of 65 mm. Building and collapse are observed at the start and finish of deposition in the constructed weldment, as shown in Fig. 2 as a result of the deposition's unidirectional deposition strategy. When the number of layers increases, the built region approaches its maximum height in comparison to the collapse region. This causes the deposited component dimensions to be inaccurate. To solve this problem, additional passes are welded at the wall's endpoint to keep the height constant between the starting and ending points.

### 3.2. Microstructural analysis

In order to comprehend the fundamental changes in phases and grain structure morphology in top and the bottom zones of the constructed weldment, a microstructural study was conducted on the sample using an Optical Microscope. In the Figs. 4(a) & 4(b), the images obtained by optical microscopy are displayed. The constructed weldment's top and bottom zones both exhibit the effective grain structure.

The variation in heat transfer between the top and bottom zones is the main cause of the variance in microstructure. The majority of the heat input during the WAAM process is

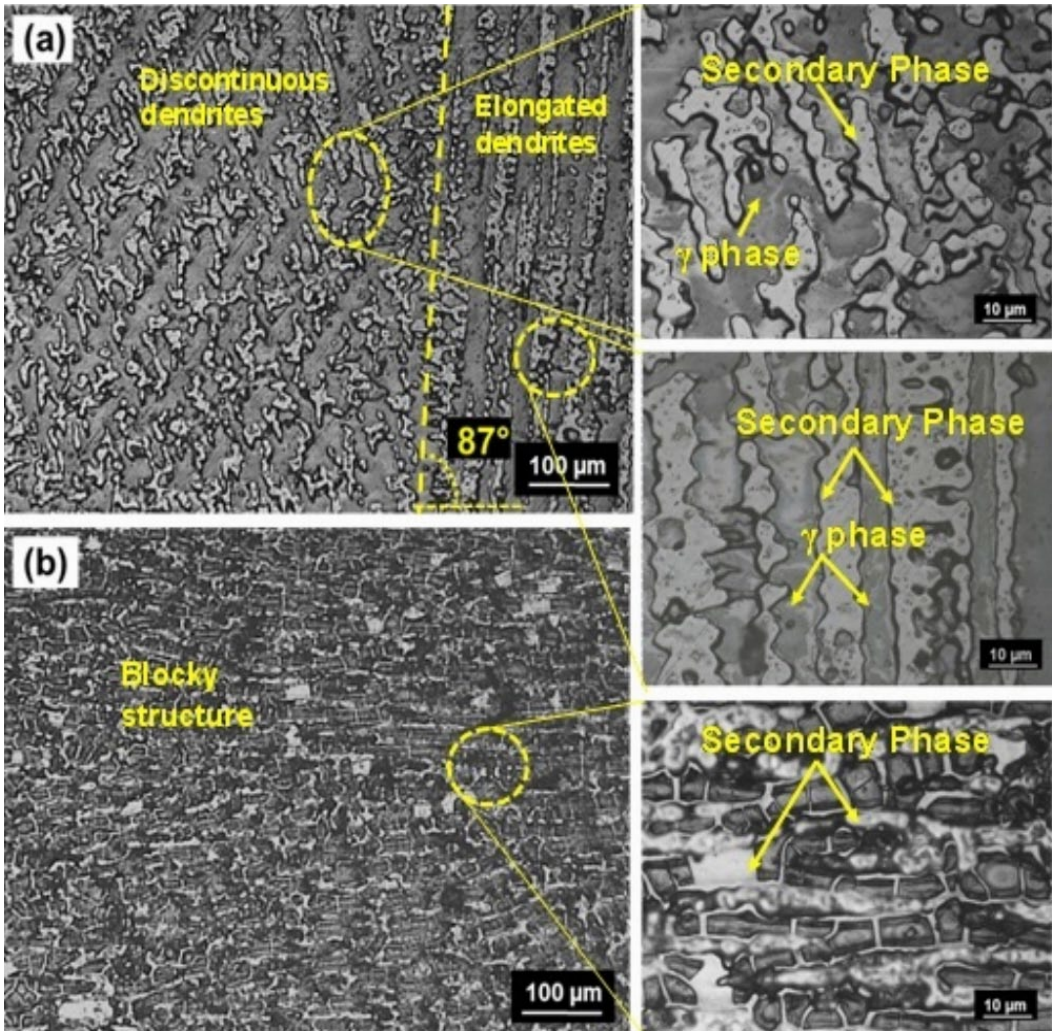


Fig. 4. (a) Optical Micrograph of the top zone (b) Optical Micrograph of the bottom zone

lost by convection and radiation to the surrounding atmosphere. Due to the quick heat transfer through the substrate plate and the high cooling rate, the top zone cools down quickly. The bottom zone, on the other hand, results in a slow rate of cooling. Due to this variation in thermal behavior during the additive welding process, the microstructures that have been observed have changed in the different regions of the deposit.

The optical microscopy in Fig. 4(a) shows that the microstructure appears to be layered, and the deposited layer is distinguished by elongated dendrites, discontinuous dendrites in the top zone due to the slow heat transfer, while Fig. 4(b) shows an equiaxed blocky structure in the bottom zone of the weldment due to the rapid heat transfer on the base plate. In addition, the formation of fine precipitates can be observed in the remelting zone of the top layer and the blocky structure formation in the bottom zone may attribute to the chill zone formation. Also, the secondary phases are found in both the top and the bottom zones of the multilayered wall built structure, and the gamma phases are found only in the top zone of the built structure.

Microstructure development and phase formation are closely related to the cooling rate of parts printed by an arc additive process. Temperature gradient G and crystallization rate V are the key factors decide the crystallization pattern. Generally, the grains grow in a preferential direction of maximum temperature gradient and the direction opposite to the direction of heat flux [19]. As depicted in Figs. 4(a) & 4(b), in the region close to the substrate, the grain size is small and shows a tendency of vertical growth. Also, the heat is lost often faster in solids than in air, and heat accumulation increases with the number of printed layers increases. The result shown in Fig. 4(a) & 4(b) envisages the presence of equiaxed crystals/ epitaxially grown dendrites in the top. As the number of layers increases, heat accumulation prone to increase and at that stage the air cooling rate become the key factor influences the microstructure development. As heat is released into the air, the molten metal pool exhibits a higher temperature gradient perpendicular to the liquid surface [20]. The bypass gas not only protects the surface of the filler metal, but also accelerates the cooling of the metal-side portion of the ingot [21]. As a result, the crystallization angle can be shifted in the direction perpendicular to the melt pool surface, and the crystal crystallized along the direction with the maximum temperature gradient of 87° affirms the same. The schematic diagram of mode of crystallization is shown in Fig. 5.

Epitaxial dendrites formation is evident in the central portion of the printed structure and the trend of microstructure development can be assumed as follows: Chill zone plane crystal → Columnar crystal → Dendrites with shorter primary arm → Dendrites with longer primary arm → Secondary dendrites. These stages of microstructure development can be further understood with the variation of undercooling. During the solidification of a molten metal, the influence of undercooling on the formation of grains and phases can be expressed by Eq. (1) [22].

$$\frac{G_L}{v} \geq \sum_{i=1}^{n} -\frac{m_{Li}\omega_i\left(1-k_i\right)}{D_{Li}k_i} \tag{1}$$

Where $G_L$ is the temperature gradient, $v$ is the crystallization rate, $m_{Li}$ is the liquidus slope, $\omega_i$ is the initial mass fraction, $D_{Li}$ is the diffusion coefficient of the element $i$ in the liquid phase and $k_i$ is the partition coefficient.

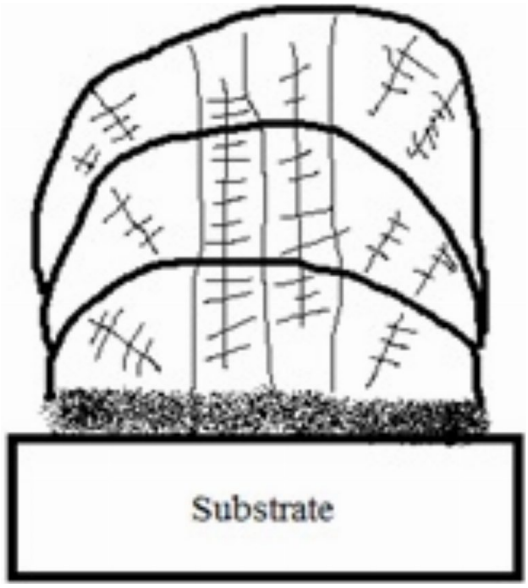


Fig. 5. Schematic micro structural development

As the layer of deposition succeeds, the heat energy of the arc accumulates in the sample and it increases the temperature of the printed sample to reduce the temperature gradient in the top surface of the molten metal pool. This subsequently slow down the cooling rate and provides longer interval for the growth of the dendrites. However, the zone close to substrate can have a high rate of heat dissipation and thus it forms a finer dendrites/ blocky structure.

### 3.3. Mechanical characteristics

On the top and the bottom zones of the weldment, to analyze the mechanical property tensile test was taken along with that fractography test was conducted in the fractured zone of the tensile specimen to correlate the results of mechanical and microstructural property.

#### 3.3.1. Tensile testing

Tensile specimens are extracted (as per ASTM E8 standard) from the top and the bottom zones of the built weldment are subjected to tensile test using a universal testing machine setup to test their tensile test properties. The tensile strength, Yield stress and Elongation of top zone-built weldment were estimated to be 571 MPa, 340 MPa, 53%. In bottom zone the tensile strength, Yield stress and Elongation was 623 MPa, 394 MPa, 57% and these values are shown in the TABLE 2. The stress strain graph for the tensile strength in both zones is shown in the Figs. 6(a) & 6(b).

According to the Hall-Petch relationship between grain size and yield strength, for a certain limit, smaller the grain size, higher will be the strength. According to the microstructure, the bottom position is expected to have higher mechanical property. However the formation of solidification can be attributed to reduction in mechanical property. The Inconel 625 alloy is susceptible to hot cracking and the temperature gradient induced stress can further accelerate the internal crack formation. This in turn may reduce the mechanical properties [23].

TABLE 2

Tested values of top & bottom zones

| Zones of multilayer wall | Tensile Strength MPa | Yield Stress MPa | Elongation % |
|---|---|---|---|
| **Top zone** | 571 | 340 | 53 |
| **Bottom zone** | 623 | 394 | 57 |

Fig. 6(a) Stress-strain graph for Top zone of the built structure (b) Stress-strain graph for bottom zone of the built structure

It is seen that the presence of dendrites leads to the deduction of the ultimate tensile strength in the top zone of the multi layered wall structure; also, it seems that the presence of cracks is visible during the fractography test, which is shown in Fig. 7(b). Whereas in the bottom zone, the presence of equiaxed blocky structure contributes the higher tensile strength than the bottom zone of the multi layered wall structure.

### 3.3.2. Fractographic testing

The results from the fractography test shows that the fracture of the specimen is under ductile mode. The images of the fractured surface was examined by using Scanning Electron Microscopy (SEM) is shown in the Figs. 7(a) & 7(b). Fractog-

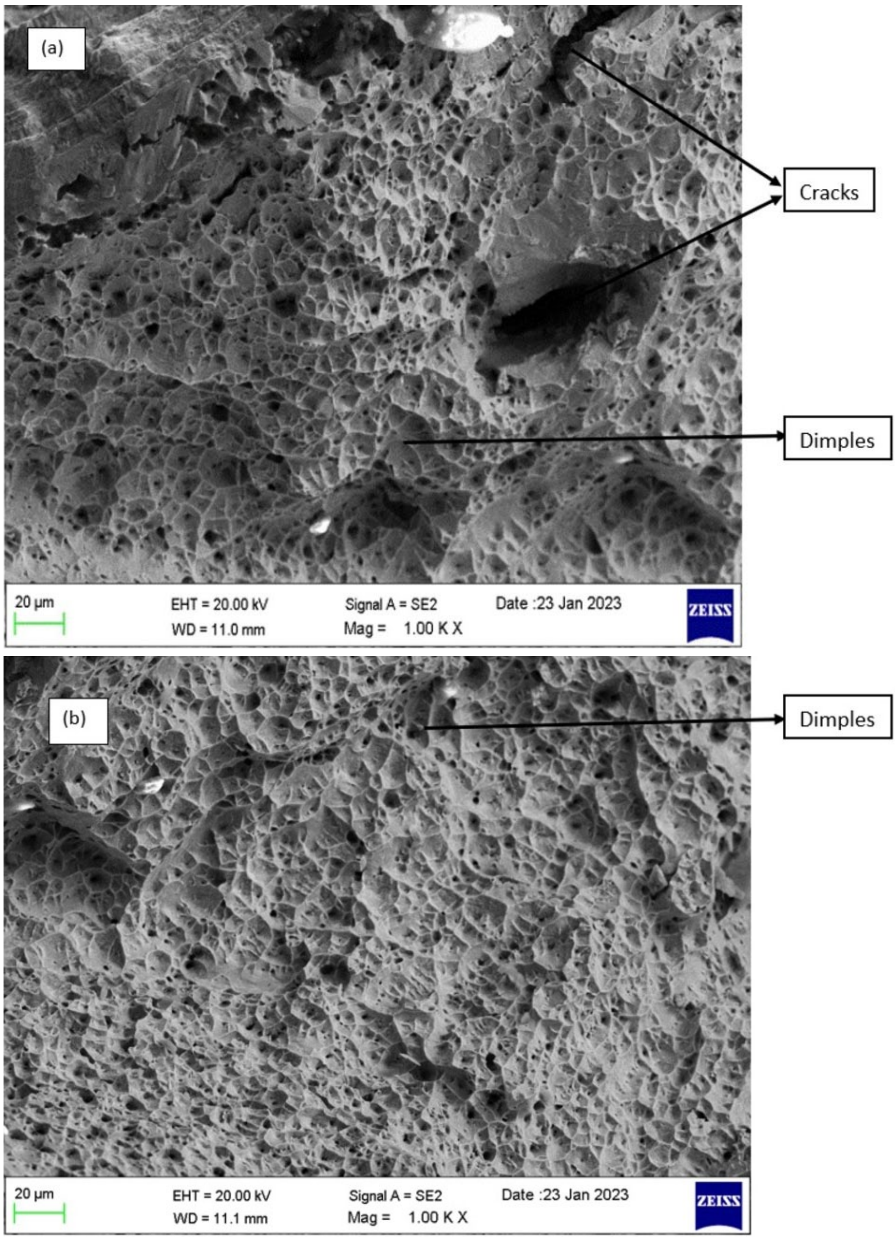


Fig. 7. (a) Fractography of top zone (b) Fractography of bottom zone

raphy test was conducted in the top and bottom zones of the multilayered wall structure using the fractured tensile specimen in order to identify the connection between the microstructure and the causes of the fracture ultimately as well as the methods of crack start and propagation.

The presence of dimples is clearly identified in both top and bottom zones fractured surface after the tensile test which indicates the ductile fracture. In the fractography of the top zone cracks are identified, this also be the reason of the decreased tensile property.

## 4. Conclusion

Using WAAM technique on GTAW process, Inconel 625 alloy was created in the current work. In the top and the bottom zones of multi-layered wall structure, the resulting microstructure and mechanical characteristics were examined, and the impact of the solidification rate on these features was discovered. The inferences that could be made include the following:

- The GTAW process, which is unidirectional welding, was used to weld the multi layered wall construction made of Inconel 625 alloy. The height at the end of the welding process is reduced as a result of unidirectional welding. Thus, additional welding passes are required at the end region to provide the required dimensional accuracy.
- Microstructure results show that the deposited bottom layer consists of a blocky structure, which is more likely equiaxed dendrites, and the top layer consists of discontinuous and elongated dendrites, this difference in microstructure is due to the different solidification rate in the top and bottom zones.
- The solidification rate at the bottom zone is very fast because the heat is conducted through the substrate. Compared to the bottom zone, the rate of solidification in the top zone is low.
- The bottom zone's tensile properties, such as tensile strength and yield strength, were 8% and 13% higher than in the top zone, respectively. The top zones ultimate tensile strength is reduced because of the presence of dendritic microstructure.
- The tensile and the fractography test results show that the presence of cracks directly influences the tensile and yield strengths of the multilayer wall structure, which leads to a deduction in the tensile and yield strength values in the top zone of the multi layered wall.

## REFERENCES


[1] H.D. Nguyen, A. Pramanik, A.K. Basak, Y. Dong, C. Prakash, S. Debnath, D. Buddhi, A critical review on additive manufacturing of Ti-6Al-4V alloy: microstructure and mechanical properties. Journal of Materials Research and Technology **18**, 4641-4661 (2022). DOI: https://doi.org/10.1016/j.jmrt.2022.04.055

[2] M.E. Korkmaz, S. Waqar, A. Garcia-Collado, M.K. Gupta, G.M. Krolczyk, "A technical overview of metallic parts in hybrid additive manufacturing industry," Journal of Materials Research and Technology, (2022).
DOI: https://doi.org/10.1016/j.jmrt.2022.02.085

[3] Z. Pan, D. Ding, B. Wu, D. Cuiuri, H. Li, J. Norrish, Arc welding processes for additive manufacturing: a review. Transactions on Intelligent Welding Manufacturing, 3-24 (2018).
DOI: https://doi.org/10.1007/978-981-10-5355-9_1

[4] M. Chintala, T. Kumar, M. Sathishkumar, N. Arivazhagan, M. Manikandan, Technology development for producing Inconel 625 in aerospace application using wire arc additive manufacturing process. Journal of Materials Engineering and Performance **30**, 7, 5333-5341 (2021).
DOI: https://doi.org/10.1007/11665-021-05781-6

[5] M. Owais, J. Mridul, W. Noor, N.H., Wire Arc Additive Manufacturing (WAAM) of Inconel 625 Alloy and its Microstructure and Mechanical Properties. International Research Journal of Engineering and Technology (IRJET) **8**, 2 (2021).

[6] H. Geng, J. Li, J. Xiong, X. Lin, F. Zhang, Optimization of wire feed for GTAW based additive manufacturing. Journal of Materials Processing Technology **243**, 40-47 (2017).
DOI: https://doi.org/10.1016/j.jmatprotec.2016.11.027

[7] X. Wang, A. Wang, K. Wang, Y. Li, Process stability for GTAW-based additive manufacturing. Rapid Prototyping Journal (2019).
DOI: https://doi.org/10.1108/RPJ-02-2018-0046

[8] P.P. Thakur, A.N. Chapgaon, A review on effects of GTAW process parameters on weld. International Journal of Research in Aeronautical and Mechanical Engineering **4**, 136-140 (2016).
DOI: https://doi.org/10.13140/RG.2.2.11535.38569

[9] S.P. Kumar, S. Elangovan, R. Mohanraj, J.R. Ramakrishna, A review on properties of Inconel 625 and Inconel 718 fabricated using direct energy deposition. Materials Today: Proceedings **46**, 7892-7906 (2021).
DOI: https://doi.org/10.1016/j.matpr.2021.02.566

[10] O.M. Akselsen, R. Bjørge, H.W. Ånes, X. Ren, B. Nyhus, Microstructure and properties of wire arc additive manufacturing of Inconel 625. Metals **12**, 11, 1867 (2022).
DOI: https://doi.org/10.3390/met12111867

[11] S.S. Kumar, C.B. Maheswaran, T.D.B. Kannan, Experimental investigation on a pulsed TIG welding of Inconel 625. Materials Today: Proceedings **45**, 2109-2114 (2021).
DOI: https://doi.org/10.1016/j.matpr.2020.09.724

[12] C. Guo, M. Ying, H. Dang, R. Hu, F. Chen, Microstructural and intergranular corrosion properties of Inconel 625 superalloys fabricated using wire arc additive manufacturing. Materials Research Express **8**, 3, 035103 (2021).
DOI: https://doi.org/10.1088/2053-1591/abe977

[13] S. Mohan Kumar, A. Rajesh Kannan, N. Pravin Kumar, R. Pramod, N. Siva Shanmugam, A.S. Vishnu, S.G. Channabasavanna, Microstructural features and mechanical integrity of wire arc additive manufactured SS321/Inconel 625 functionally gradient material. Journal of Materials Engineering and Performance **30**, 8, 5692-5703 (2021).
DOI: https://doi.org/10.1007/11665-021-05617-3

[14] G. Ravi, N. Murugan, R. Arulmani, Microstructure and mechanical properties of Inconel-625 slab component fabricated by wire arc additive manufacturing. Materials Science and Technology **36**, 16, 1785-1795 (2020).
DOI: https://doi.org/10.1080/02670836.2020.1836737

[15] E. Karayel, Y. Bozkurt, Additive manufacturing method and different welding applications. Journal of Materials Research and Technology **9**, 5, 11424-11438 (2020).
DOI: https://doi.org/10.1016/j.jmrt.2020.08.039

[16] G.N. Ahmad, M.S. Raza, N.K. Singh, H. Kumar, Experimental investigation on Ytterbium fiber laser butt welding of Inconel 625 and Duplex stainless steel 2205 thin sheets. Optics and Laser Technology **126**, 106117 (2020).

[17] J. Sivakumar, M. Vasudevan, N.N. Korra, Systematic welding process parameter optimization in activated tungsten inert gas (A-TIG) welding of Inconel 625. Transactions of the Indian Institute of Metals **73**, 3, 555-569 (2020).
DOI: https://doi.org/10.1016/j.optlastec.2020.106117

[18] V. Dhinakaran, J. Ajith, A.F.Y. Fahmidha, T. Jagadeesha, T. Sathish, B. Stalin, Wire Arc Additive Manufacturing (WAAM) process of nickel based superalloys – A review. Materials Today: Proceedings **21**, 920-925 (2020).
DOI: https://doi.org/10.1016/j.matpr.2019.08.159

[19] H.Y. Wan, Z.J. Zhou, C.P. Li, G.F. Chen, G.P. Zhang, Effect of scanning strategy on grain structure and crystallographic texture of Inconel 718 processed by selective laser melting. Journal of Materials Science and Technology **34**, 10, 1799-1804 (2018).

[20] F.E. Bock, J. Herrnring, M. Froend, J. Enz, N. Kashaev, B. Klusemann, Experimental and numerical thermo-mechanical analysis of wire-based laser metal deposition of Al-Mg alloys. Journal of Manufacturing Processes **64**, 982-995 (2021).
DOI: https://doi.org/10.1016/j.jmapro.2021.02.016

[21] F. Montevecchi, G. Venturini, N. Grossi, A. Scippa, G. Campatelli, Heat accumulation prevention in Wire-Arc-Additive-Manufacturing using air jet impingement. Manufacturing Letters **17**, 14-18 (2018).

[22] Y. Shen, J. Liu, S. Yang, B. Yan, Y. He, H. Liu, H. Xu, Dendrite growth behavior in directionally solidified Fe-C-Mn-Al alloys. Journal of Crystal Growth **511**, 118-126 (2019).

[23] L. Karlsson, E.L. Bergquist, S. Rigdal, N. Thalberg, in: T. Böllinghaus, H. Herold, C.E. Cross, J.C. Lippold (eds), Evaluating Hot Cracking Susceptibility of Ni-Base SAW Consumables for Welding of 9% Ni Steel. Hot Cracking Phenomena in Welds II, Springer, Berlin, Heidelberg, (2008).
DOI: https://doi.org/10.1007/978-3-540-78628-3_17